Supplemental material: Out-of-time-ordered-correlator quasiprobabilities robustly witness scrambling

José Raúl González Alonso,[1,*] Nicole Yunger Halpern,[2] and Justin Dressel[1,3]

[1] *Schmid College of Science and Technology, Chapman University, Orange, CA 92866, USA*
[2] *Institute for Quantum Information and Matter, Caltech, Pasadena, CA 91125, USA*
[3] *Institute for Quantum Studies, Chapman University, Orange, CA 92866, USA*

(Dated: November 1, 2018)

OTOC MEASUREMENT PROTOCOLS AND NUMERICAL SIMULATIONS

Here, we provide more details about the numerical procedure used to simulate each OTOC-measurement protocol. For each protocol, the time-evolution implementation changes, depending on whether we are simulating a closed or an open system. In the case of a closed system, the forward time evolution amounts to applying the unitary $U(t)$ generated by the appropriate Hamiltonian. For the open system, we evolve a given operator O by

$$O \mapsto dt \sum_i \gamma_i L_i U(dt) O U(dt)^\dagger L_i^\dagger + L_0 U(dt) O U(dt)^\dagger L_0^\dagger. \tag{S1}$$

where $L_0 = \sqrt{\mathbb{1} - dt \sum_i \gamma_i L_i^\dagger L_i}$ and the L_i's are the Lindblad operators associated with the decoherence. In our case, the Lindblad operators represent individual-qubit dephasing. The backward time evolution flips the sign of t only for the unitary evolution, i.e., $U(t) \leftrightarrow U^\dagger(t)$. This method ensures state positivity, unlike more direct methods for integrating the master equation. It is also possible to construct a superoperator matrix to simulate the dynamics of the system, even if decoherence is present. However, because of memory constraints, and the lack of symmetries with which to simplify the problem, this method becomes impractical even for a modest number of qubits.

In what follows, we detail the numerical procedures used to simulate the measurement protocols outlined in Refs. [S1–S4]. Note that in our numerical procedures we only simulate the decoherence accumulated in each protocol but, for simplicity, ignore other experimental imperfections.

Weak-measurement protocol

To calculate $\mathrm{Tr}\,(ABCD\rho)$, we implement the procedure outlined below, based on [S1, S2]. One advantage of the weak-measurement protocol is that we can use it to calculate either the OTOC quasiprobability $\tilde{p}_t(v_1, w_2, v_2, w_3)$ (by using the projectors onto eigenspaces, $A = \Pi_{w_3}^W, B = \Pi_{v_2}^V, C = \Pi_{w_2}^W$, and $D = \Pi_{v_1}^V$) or the OTOC $F(t)$ (with $A = W(t)^\dagger, B = V^\dagger, C = W(t)$, and $D = V$). The unitary evolution is generated by the system Hamiltonian tensored with identity operators on the ancillas required by the protocol. The steps in the calculation are as follows:

1. Prepare ρ.
2. Left-multiply by D.
3. Evolve the result forward in time by t units.
4. Left-multiply the result by C.
5. Evolve the result backward in time by t units.
6. Left-multiply the result by B.
7. Evolve the result forward in time by t units.
8. Left-multiply the result by A, and take the trace to obtain $F(t)$ or $\tilde{p}_t(v_1, w_2, v_2, w_3)$.

While taking the trace is a trivial operation in theory, in an experiment, it is necessary to repeat the procedure outlined above multiple times and calculate the average of the outcomes, using their relative frequencies to then obtain the trace. Similarly, a left or right multiplication involves a weak coupling to an ancilla followed by the measurement of an appropriate observable on the ancilla. For explicit examples on how to do this with qubits see Ref. [S5].

Interferometric protocol

The Swingle *et. al.* interferometric protocol [S3] uses an ancilla to apply different operators selectively. On one branch of an interferometer the product of the operators V and $W(t)$ is applied. Meanwhile, on the other branch, the product in reversed order is applied. The unitary evolution is generated by the system Hamiltonian tensored with an identity operator on the ancilla that creates the interferometric branching. We have used the following numerical procedure:

1. Prepare $\rho \otimes |+\rangle\langle+|$.
2. Apply $\mathbb{1} \otimes |0\rangle\langle 0| + V \otimes |1\rangle\langle 1|$.
3. Evolve the result forward in time by t units.
4. Apply $W \otimes \mathbb{1}$ to the result.

5. Evolve the result backward in time by t units.
6. Apply $V \otimes |0\rangle\langle 0| + \mathbb{1} \otimes |1\rangle\langle 1|$.
7. Measuring the control qubit in the σ_x or the σ_y eigenbasis yields $\mathrm{Re}\, F(t)$ or $\mathrm{Im}\, F(t)$ respectively.

Quantum-clock protocol

Finally, the Zhu *et. al.* quantum-clock protocol [S4], like the Swingle *et. al.* interferometric protocol, relies on an ancilla to selectively apply the product of W and V in different orders to each branch. However, the unitary evolution is generated by the system Hamiltonian H tensored with a σ_z on said ancilla, i.e., the total Hamiltonian is $H_T = H \otimes \sigma_z$. The advantage of this procedure is that the ancilla also controls the direction of time evolution. In other words, H_T generates a unitary of the form

$$U_T(t) = U(t) \otimes |0\rangle\langle 0| + U(-t) \otimes |1\rangle\langle 1| \,. \tag{S2}$$

The numerical procedure we used in this case is outlined below:

1. Prepare $\rho \otimes |+\rangle\langle +|$
2. Apply $\mathbb{1} \otimes |0\rangle\langle 0| + V \otimes |1\rangle\langle 1|$.
3. Evolve in time by t units.
4. Apply $\mathbb{1} \otimes |0\rangle\langle 0| + W \otimes |1\rangle\langle 1|$.
5. Apply $\mathbb{1} \otimes \sigma_x$.
6. Evolve in time by $2t$ units.
7. Apply $\mathbb{1} \otimes \sigma_x$.
8. Apply $W \otimes |0\rangle\langle 0| + \mathbb{1} \otimes |1\rangle\langle 1|$.
9. Evolve in time by t units.
10. Apply $V \otimes |0\rangle\langle 0| + \mathbb{1} \otimes |1\rangle\langle 1|$.
11. Measuring the clock qubit in the σ_x or the σ_y eigenbasis yields $\mathrm{Re}\, F(t)$ or $\mathrm{Im}\, F(t)$, respectively.

CHANGES IN THE BEHAVIORS OF $\tilde{t}_*$, t_m, AND t_z AS h/J VARIES

In the main text, we analyzed the behaviors of three different time scales in the total nonclassicality $\tilde{N}(t)$ of the quasiprobability $\tilde{p}_t$, for two values of h/J. All these time scales are analyzed up to numerical imprecisions given by the square of the time step Δt used in the simulations. The definitions of the time scales are given below:

1. $\tilde{t}_*$, the time at which $\tilde{N}(t)$ first deviates from zero.
2. t_m, the time at which $\tilde{N}(t)$ attains its first local maximum.
3. t_z, the time at which $\tilde{N}(t)$ first returns to zero after the first maximum.

We saw that, even in the presence of decoherence, the asymmetry between $t_m - \tilde{t}_*$ and $t_z - t_m$ distinguished between the integrable ($h/J = 0$) and nonintegrable ($h/J \neq 0$) cases. In the plots below, we analyze the behaviors of the time scales for 15 equally spaced values of h/J between 0.0 and 0.5.

First, we present an example of the effects that changing h/J has on the total nonclassicality $\tilde{N}(t)$. As we can see in Fig. S1, as the value of h/J increases, so does the cumulative total nonclassicality. This feature is independent of decoherence. Hence, we can think of h/J as a parameter that controls not only the scrambling nature of the Hamiltonian but also the cumulative behavior of the total nonclassicality $\tilde{N}(t)$. For instance, we see a sharp transition in t_z at $h/J = 0$: $\tilde{N}(t)$ for the integrable case promptly returns to zero after its first maximum but takes longer for all the nonintegrable cases. This behavior is expected since $h/J = 0$ indicates when the system is integrable.

We illustrate our conjecture using different values of h/J in Fig. S2, where we plot the ratio $(t_z - t_m)/(t_m - \tilde{t}_*)$ as a function of h/J. We interpret the quantity $t_z - t_m$ as a measure of how long it takes for some quantum information in the system to recollect, whereas $t_m - \tilde{t}_*$ indicates the time to achieve maximal quasiprobability nonclassicality. Therefore, their ratio is a measure of how asymmetrical the first peak in the total nonclassicality $\tilde{N}(t)$ is. There is a noticeable difference between the integrable and nonintegrable cases: For the decoherence-free case, there is a discontinuous transition where the recollection time $t_z - t_m$ becomes longer than the simulation time for $h/J > 0$. Adding decoherence softens this transition. The ratio remains of order 1 for a wider range of small h/J, in accordance with the expectation of integrability, before a sharp but smooth transition to a ratio that is over an order of magnitude larger, in accordance with the expectation of non-integrability.

To gain further insights into the behavior of the ratio $(t_z - t_m)/(t_m - \tilde{t}_*)$, we additionally study the behavior of each of the time scales $\tilde{t}_*$, t_m, and t_z separately. Figure S3 shows that $\tilde{t}_*$, the point at which $\tilde{N}(t)$ first deviates from zero, is hardly affected by changes in h/J. To compute $\tilde{t}_*$ in our simulations, we detected the first deviation from a bound set by the square of the time step Δt used in our numerical simulations. However, as Fig. S3 shows, the onset of nonclassicality is delayed by decoherence. This is to be expected, since, in the presence of decoherence, it is more difficult for the system to build the coherence responsible for nonclassical behavior. Furthermore, for a fixed value of h/J, systems with an infinite-temperature initial Gibbs state tend to have values of $\tilde{t}_*$

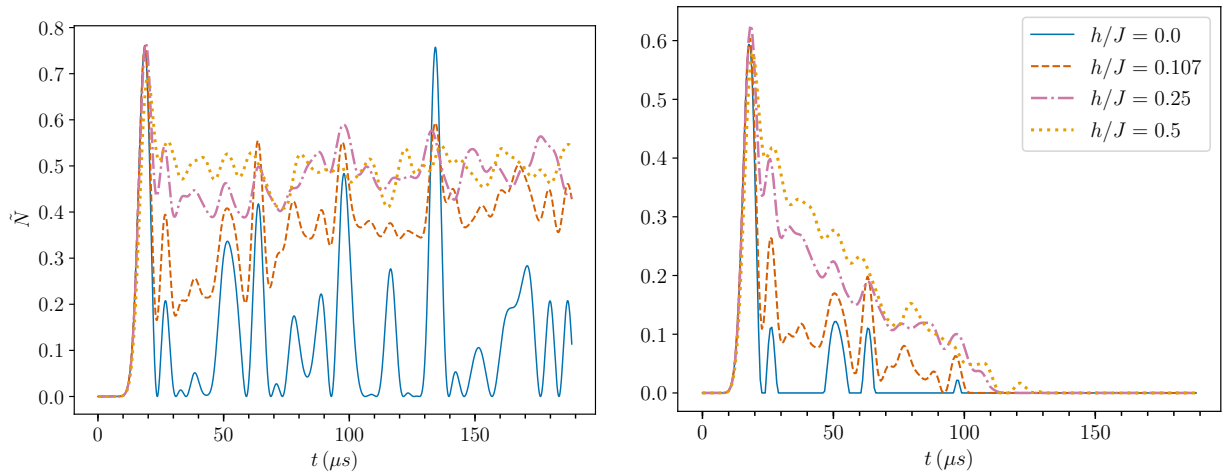

(a) Ideal case (b) Decoherent case

Figure S1. Behavior of $\tilde{N}(t)$ for different values of h/J for the (a) ideal and (b) decoherent cases with an initial infinite-temperature Gibbs state, $\mathbb{1}/2^N$. In the decoherent case, the system undergoes environmental dephasing of each qubit with a decay constant of $T_2^* = 130\ \mu s$. The local operators are $W = \sigma_1^z$ and $V = \sigma_N^z$. These plots highlight how h/J controls not only integrability and scrambling, but also cumulative nonclassicality.

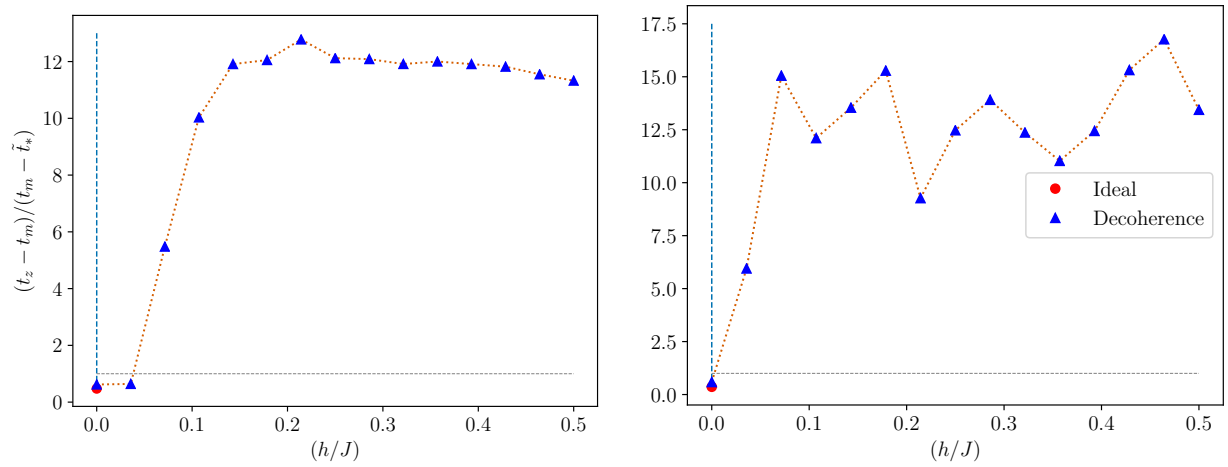

(a) Infinite temperature (b) Finite temperature

Figure S2. Behavior of the ratio $(t_z - t_m)/(t_m - \tilde{t}_*)$ as a function of h/J for the (a) infinite-temperature and (b) finite-temperature initial Gibbs states, $e^{-H/T}/Z$, with and without decoherence. Recall that t_z is longer than the total simulation time for all the decoherence-free nonintegrable cases ($h/J \neq 0$). Therefore, the only ideal (decoherence-free) case we report is integrable ($h/J = 0$).

larger than their counterparts with a finite-temperature initial Gibbs state. The infinite-temperature state is initially diagonal in the eigenblocks of W and V and therefore requires more time to build quantum coherences than the finite-temperature state.

Next, in Fig. S4, we present the behavior of the point in time, t_m, at which the first maximum in $\tilde{N}(t)$ as a function of h/J occurs. Decoherence decreases the time required to reach the first maximum. This is reasonable, since decoherence overall dampens the nonclassicality and therefore reduces the value of the maximum. Hence, it becomes easier for the system to reach the smaller value of $\tilde{N}(t)$ in a shorter amount of time. t_m depends on the system dynamics and the initial state. We can appreciate an interesting difference in the plots corresponding to different choices of initial state. Whereas the curves corresponding to the infinite-temperature initial Gibbs states show a monotonic behavior, the ones

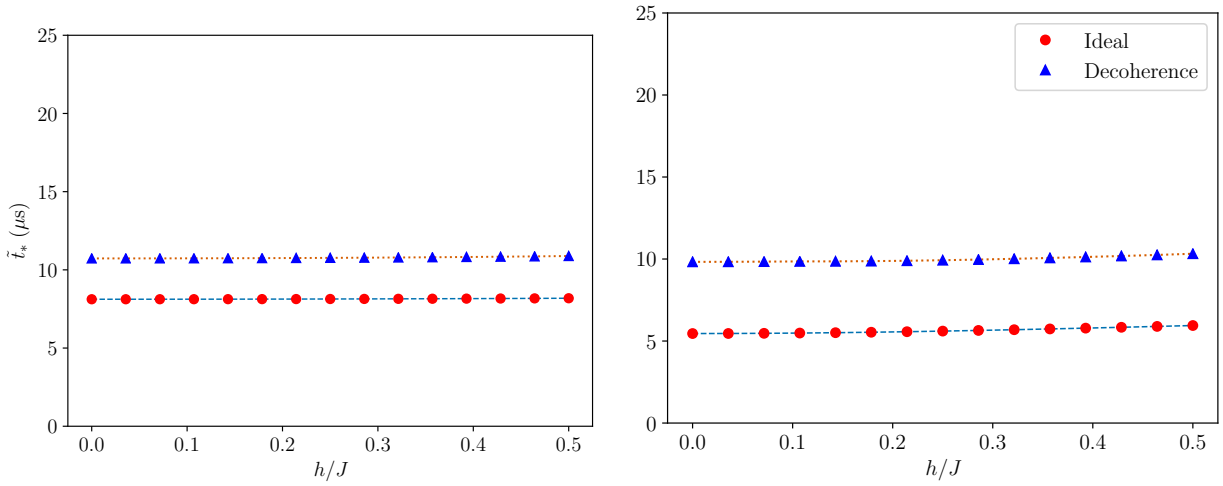

(a) Infinite temperature

(b) Finite temperature

Figure S3. Behavior of $\tilde{t}_*$, the point at which $\tilde{N}(t)$ first deviates from zero, as a function of h/J for the (a) infinite-temperature and (b) finite-temperature initial Gibbs states, with and without decoherence. Simulation parameters are similar to those in previous examples.

for the finite-temperature initial Gibbs states briefly rise and then fall. Further understanding of this particular behavior is left for future research.

Finally, in Fig. S5, we observe how the time t_z to the the subsequent zero after the first maximum changes with h/J. As expected, without decoherence, only $h/J = 0$ reaches zero again in a time shorter than the total simulation time, i.e., the maximum value of t for which we calculated $F(t)$, $\tilde{p}_t$, and $\tilde{N}(t)$. However, this changes with the addition of decoherence. With it, t_*, the time to reach zero again, is shorter than the total simulation time for all cases. However, t_* is significantly longer for the nonintegrable cases, regardless of the choice of initial state.

* Corresponding author: gonzalezalonso@chapman.edu

[S1] N. Yunger Halpern, "Jarzynski-like equality for the out-of-time-ordered correlator," Physical Review A **95**, 012120 (2017), arXiv:1609.00015.

[S2] N. Yunger Halpern, B. Swingle, and J. Dressel, "Quasiprobability Behind the Out-of-Time-Ordered Correlator," Physical Review A **97**, 042105 (2018).

[S3] B. Swingle, G. Bentsen, M. Schleier-Smith, and P. Hayden, "Measuring the scrambling of quantum information," Physical Review A **94**, 040302 (2016), arXiv:1602.06271.

[S4] G. Zhu, M. Hafezi, and T. Grover, "Measurement of many-body chaos using a quantum clock," Physical Review A **94**, 062329 (2016), arXiv:1607.00079.

[S5] J. Dressel, J. R. González Alonso, M. Waegell, and N. Yunger Halpern, "Strengthening weak measurements of qubit out-of-time-order correlators," Physical Review A **98**, 012132 (2018), arXiv:1805.00667.

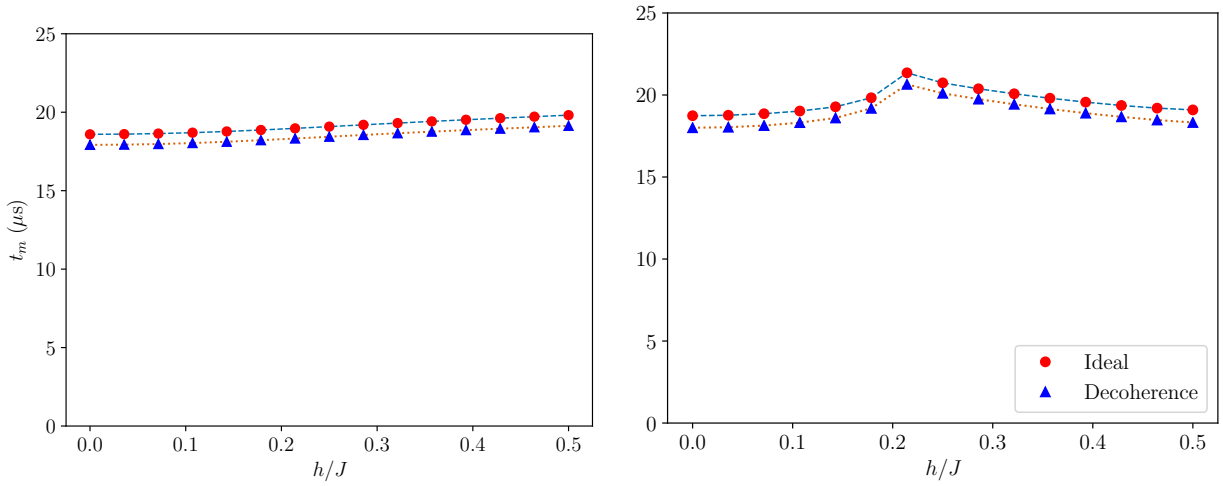

(a) Infinite temperature (b) Finite temperature

Figure S4. Behavior of t_m, the point at which $\tilde{N}(t)$ reaches its first local maximum, as a function of h/J for the (a) infinite-temperature and (b) finite-temperature initial Gibbs states, with and without decoherence.

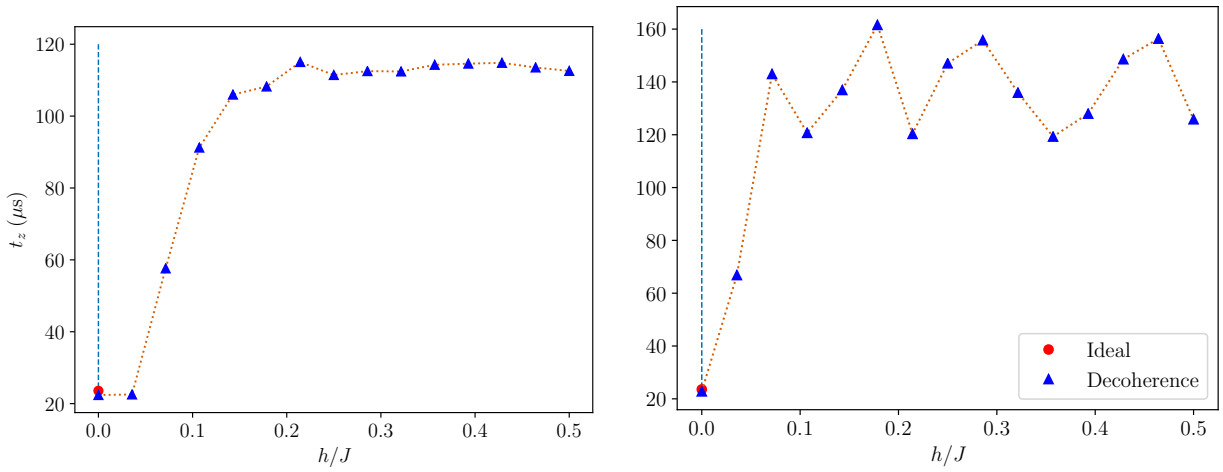

(a) Infinite temperature (b) Finite temperature

Figure S5. Behavior of t_z, the point at which $\tilde{N}(t)$ reaches a subsequent zero after t_m, as a function of h/J for the (a) infinite-temperature and (b) finite-temperature initial Gibbs states with and without decoherence. For all the nonintegrable cases ($h/J \neq 0$) without decoherence, t_z was longer than the total simulation time.